Analysis of microseismicity at a mountain site

Zuolin Chen, Robert R. Stewart and Henry C. Bland

ABSTRACT

Data from a six-station seismic network provide the first detailed information on microseismicity in the vicinity of Turtle Mountain, Southern Alberta. A network of seismometers on Turtle Mountain collected data between 1986 and 1996. During this time, 121 local seismic events were located. We analyse these events, making note of their location, magnitude and the direction of first motion at each seismometer station. Results of the analysis show magnitudes varying from $M_{F\text{-}P}$ -1.3 to about 1.0. We analyse the direction of first motion for each arrival, and classify these arrivals into a set of direction patterns depending on whether the microseism was upgoing or downgoing at each of the monitoring sites. When pattern symbols are placed on a map at the seismic events' hypocenter, we find there is some correlation to the underlying geology. These pattern-maps suggest possible focal mechanisms responsible for the seismicity. If we consider the distribution of the microseismic events, topography, the post-mining weaknesses and local geology we conclude that the seismicity is likely associated with a tectonic process operating on the geological weaknesses.

INTRODUCTION

Early and recent geological studies suggest that the 1903 Frank landslide at Turtle Mountain in southern Alberta (McConnel and Brock, 1904; Allan, 1933; Jones, 1993; Benko and Stead, 1998) can be attributed to be the following four factors: the anticlinal structure with an steeply-dipping bedding planes, the undermining of the base of Turtle Mountain by the Frank coal mine, heavy rain and freezing cycles before the landslide, and an earthquake tremor in 1901. Monitoring the present microseismic activity at Turtle Mountain can provide direct evidence for the movement of fractures, coal mining influence, and thus may help distinguish causes of the grand landslides. Microseismic monitoring in the Turtle Mountain area was carried out from June to September of 1981 by the Pacific Geosciences Centre[1] using a single monitoring station (Weichert and Horner, 1981). During this period, three swarms of local microseisms were detected, but not located due to the limitation of having a single observation station. It was possible to conclude from the initial monitoring effort that the seismic events were localized and of small magnitude. A more comprehensive effort to evaluate the local seismicity was completed by deploying a six-station seismic monitoring network on the eastern flank of Turtle Mountain by Alberta Environment. This installation recorded seismic data from November of 1986 to June 1995 (Bingham, 1996).

In this paper, we examine the distribution of the hypocenter locations, magnitudes, and possible focal mechanisms of the local events recorded by the six-station seismic network. As a preliminary result, we confirm the existence of microseismic activity in and around Turtle Mountain. Measurement of the magnitudes of the events shows that only small-scaled microearthquakes less than $M_{F\text{-}P}$ 1 occurred adjacent to the study areas during the

[1] Earth Physics Branch, Energy Mines & Resources

ten-year observation period. By comparing the distribution of the several intensive seismic areas with the local topography, thrust faults and fractures, remaining coal mining and geological structure, we found that the microseismic activity might correspond to various processes of a tectonic nature. By examining the focal mechanisms of the events we show that several types of fracture movements are apparent close to the eastern slope of Turtle Mountain. In addition, we see a relation between the circular-shaped fractures, located between Turtle Mountain's North and South Peaks, and the spatial distribution of intensive seismic activity. We propose that this activity is indicative of an active fracture zone near detachment face of Turtle Mountain. Due to air-gap between the northern part of the circular fractures and the monitoring seismometers, it is difficult to know how much seismicity occurs in this area. We propose further monitoring on all sides of the circular fractures to help better understand the motion of the mountain.

SEISMIC NETWORK AND DATA PROCESSING

A seismic network, consisting of six vertical channel stations was deployed by Alberta Environment in 1986. The network was installed to for monitor local seismicity in Turtle Mountain and the immediate vicinity. This network was operational until 1995 and provides a rich archive of seismic data from Turtle Mountain. The array was replaced by a new monitoring system in 2003. The new system was installed by Emergency Management Alberta, and is now operated by the Alberta Geological Survey[2]. Data from the 2003 monitoring system was not used as part of this study.

The six-station monitoring network was formed from two arrays named FARM and FRANK. The FARM array consisted of three seismometers located about 1.5 km southeast of the South Peak of Turtle Mountain. It included stations denoted TMA, TMB and TMC. The FRANK array consisted of three seismometers located on the eastern slope of Turtle Mountain, and comprised stations denoted TMD, TME and TMF. The locations and elevations of the stations are shown in Table 1 and Figure 1. All six stations used a single short period (1 sec) Teledyne Geotech S-500 seismometer, and all were synchronized in time. In this paper, the local seismic events recorded between November of 1986 and June 1995 were processed and analyzed.

Table 1. Seismic arrays and station locations. Locations are given in the 3 degree Transverse Mercator coordinate system (3TM) with the central meridian at 114º W. The vertical reference is sea level. For convenience, the origin of the coordinate origin is shifted to x=-30870 m, and y = 5491500 m, and z = 2200m vertically (the approximate elevation of Turtle Mountain's South Peak).

array	Station code	*x* (m)	*y* (m)	z (m)	shifted *x* (m)	shifted *y* (m)	depth (m)
FRANK	TMD	-28869.091	5493562.67	1541	2000.91	2062.67	659
	TME	-29433.437	5493048.30	2018	1436.56	1548.30	182
	TMF	-28842.527	5492973.93	1643	2027.47	1473.93	557
FARM	TMA	-28303.577	5491878.16	1381	2566.42	378.16	819
	TMB	-28285.538	5492096.06	1399	2584.46	596.06	801
	TMC	-28156.685	5491948.70	1382	2716.32	448.70	818

[2] Project contact: Corey Froese, Groundwater and Geohazards Section, Alberta Geological Survey, Alberta Energy and Utilities Board

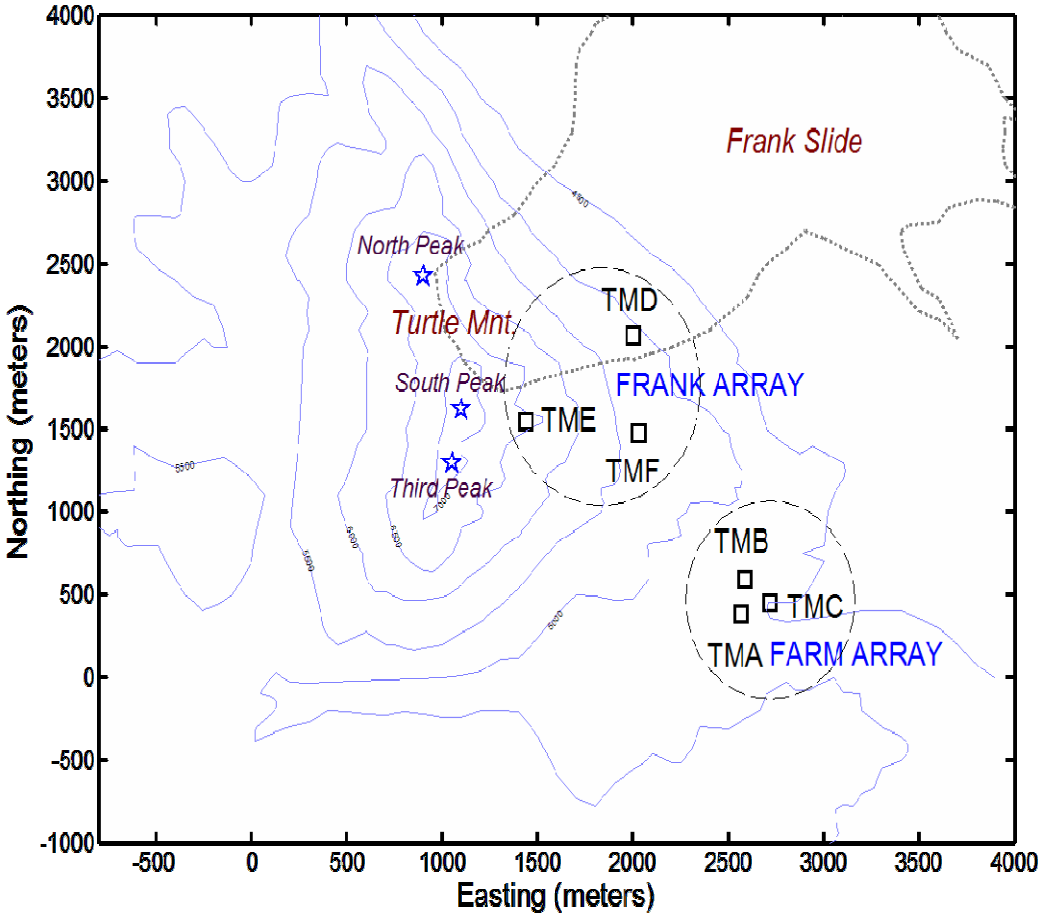

Figure 1. Map of the Turtle Mountain area and the locations of the seismic network. Open squares indicate the seismic stations; five-point stars mark the positions of the peaks of Turtle Mountain. FRANK and FARM arrays are enclosed by dashed circles.

PICKING OF P, S FIRST ARRIVALS

The accuracy of the hypocenter location highly depends on the picking precision of first arrivals of P and S-waves. Although a total of 350 local seismic events are detected (Bingham, 1986), only 153 impulsive events are recorded with at least four identifiable first arrivals of P or S waves from three or more stations of the network.

The picking precision of first arrivals of P-waves from the digital seismograms is of the order of sampling interval (0.005 seconds). Generally, the 90% error extent of the first arrival of the P-waves is regarded to be ±0.005 seconds.

As the first arrival of S-waves is often superimposed by the coda of a preceding P-wave, it may be difficult to determine the onset of the shear event precisely. The identification of the first arrival of S-waves is accomplished by using its distinguishing characteristics: lower frequencies and higher amplitude than the P-wave coda waves. The S-wave arrival often appears as an abrupt phase change and we see coincident phase

changes on multiple seismograms (Figure 2). Due to the difficulty of determining the S-wave arrival time, we estimate that 90% of the time the S-wave first arrival time is accurate to ±0.050 s.

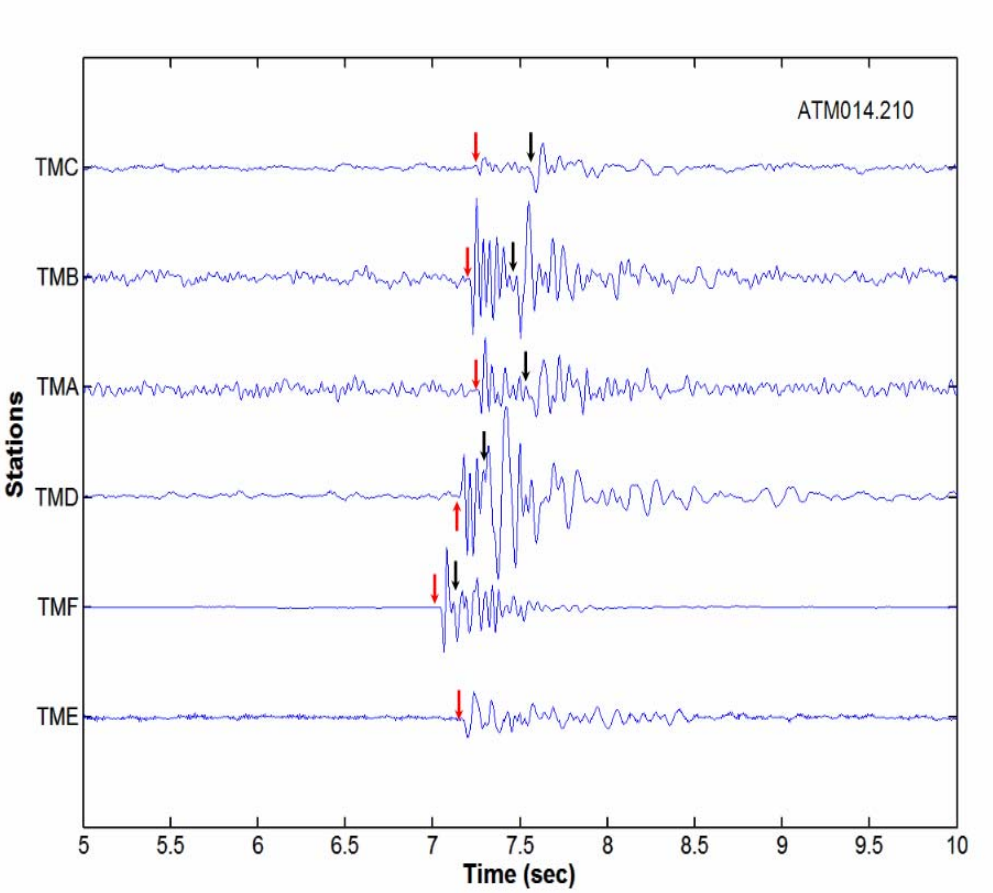

Figure 2. Example seismograms of a microseismic event recorded in September, 1991 by the FRANK and FARM arrays. Stations codes are shown at the left beginning of each recording. The arrival times of P and S-waves are indicated by red and black arrow respectively. The first arrival of S-waves is unidentified at the station TME.

HYPOCENTER LOCATION AND VELOCITY MODEL

The hypocenter locations of the local seismic events were determined using a well-known computer program called HYPOMH (Hirata & Matsu'ura, 1987). The algorithm utilised by HYPOMH is based on both observed and prior data from a Bayesian point of view. Marginal probability density function (PDF) is defined to eliminate the origin time from the location problem; the posterior PDF of hypocenter parameters is integrated over the whole range of origin time. The best estimate of the hypocenter location defines a set of spatial coordinates which maximizes the PDF. These coordinate estimates are assumed to have Gaussian error distributions. Estimation errors are evaluated by an asymptotic covariance matrix with an asymptotic posterior PDF. The program requires a one-dimensional P and S-wave velocity model, the co-ordinates of network stations, and the P and S-wave arrival times; station corrections are optional.

Velocity model

A homogeneous velocity model with a P velocity of 4.7 km/s and a V_P/V_S ratio of 1.73 was introduced to locate hypocenters. These rock parameters were mainly determined using in-situ hammer-seismic measurements and ultrasonic analysis of hand-samples (Bland et al., 2003). The zero reference level of the velocity model is set at 2200 m of elevation above sea level, which is approximately the height of the South Peak of Turtle Mountain. The initial point for searching the locations of the events is assigned at TME station, and the searching extent is 6.6 x 6.6 km laterally, 0-5 km vertically.

Reliability of hypocenter locations

A total of 84 local events are locatable by the network, and 60 local events can be located by the FRANK array. To constrain the spatial reliability of the hypocenter locations, events with lateral and vertical one-standard deviation error larger than 400 meters are removed from this study. As a result, 73 events located by the network and 48 events by the FRANK array qualified this pre-condition, and are selected for the further analysis (Figure 3 through Figure 6). Besides the 121 well-located events, four microseismic swarms are located below the Frank Slide debris by either the network or FRANK array with large lateral or vertical errors (generally about 1000 meters), and will be discussed separately.

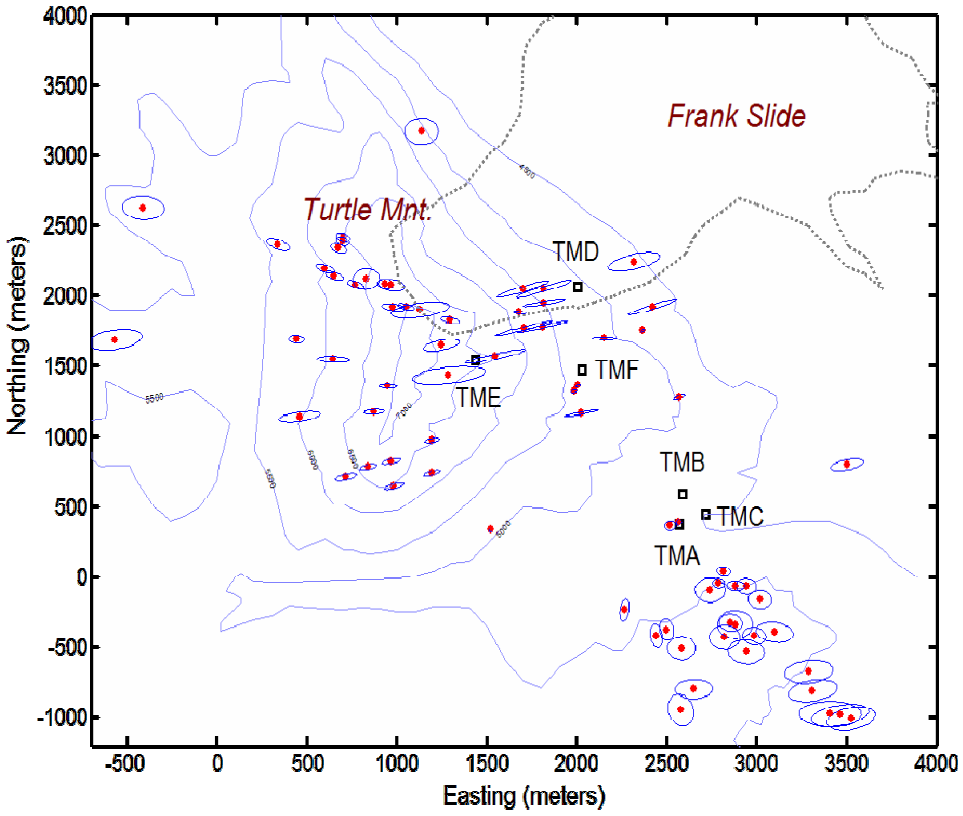

Figure 3. Lateral distribution of hypocenters (red dots) and corresponding one-standard deviation error ellipses of earthquakes located by the network. Stations are marked by black open squares. The map shows the major contours of Turtle Mountain and its vicinity. The boundary of Frank Slide debris is enclosed by a dash-dotted line. Elevations are shown in feet.

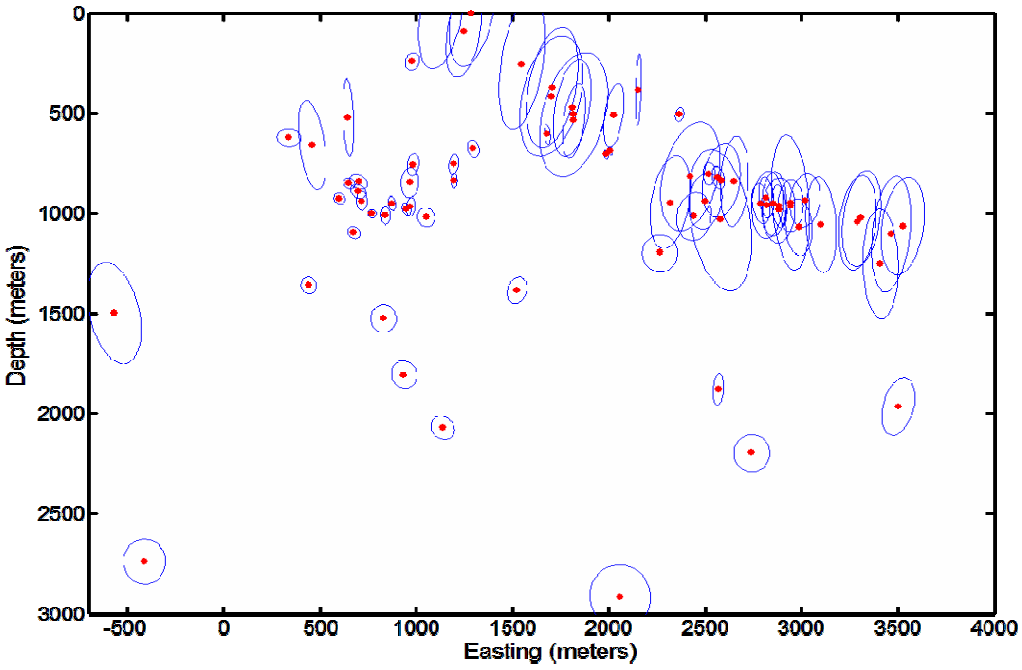

(a)

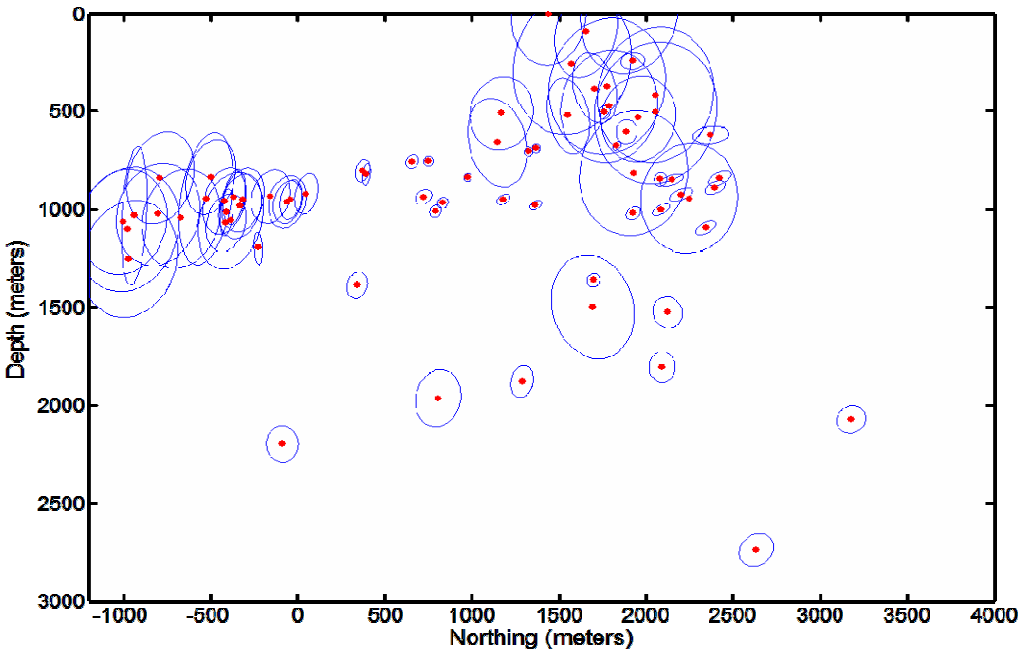

(b)

Figure 4. (a) Vertical (Easting-Depth) distribution of the hypocenters (red dots) and corresponding one-standard deviation error ellipses of earthquakes located by the network. (b) Vertical (Northing-Depth) distribution of the hypocenters (red dots) and corresponding one-standard deviation error ellipses of earthquakes located by the network.

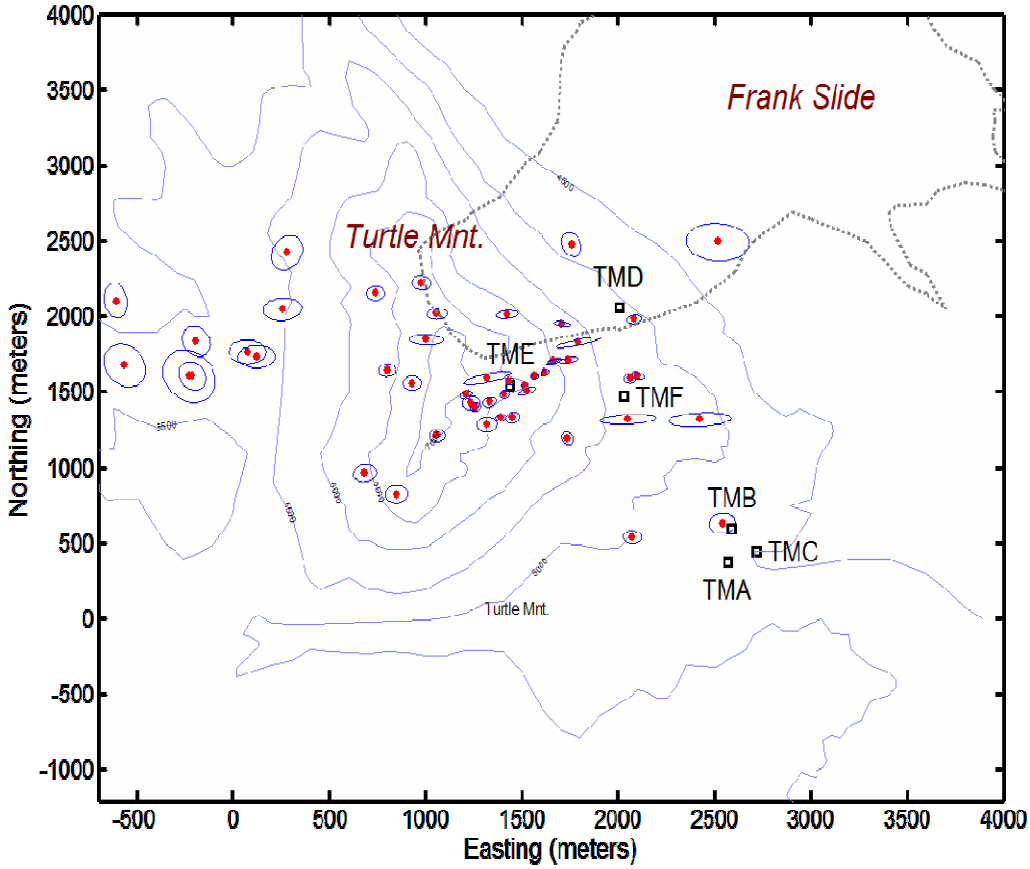

Figure 5. Lateral distribution of hypocenters (red dots) and corresponding one-standard deviation error ellipses of earthquakes located by the FRANK array.

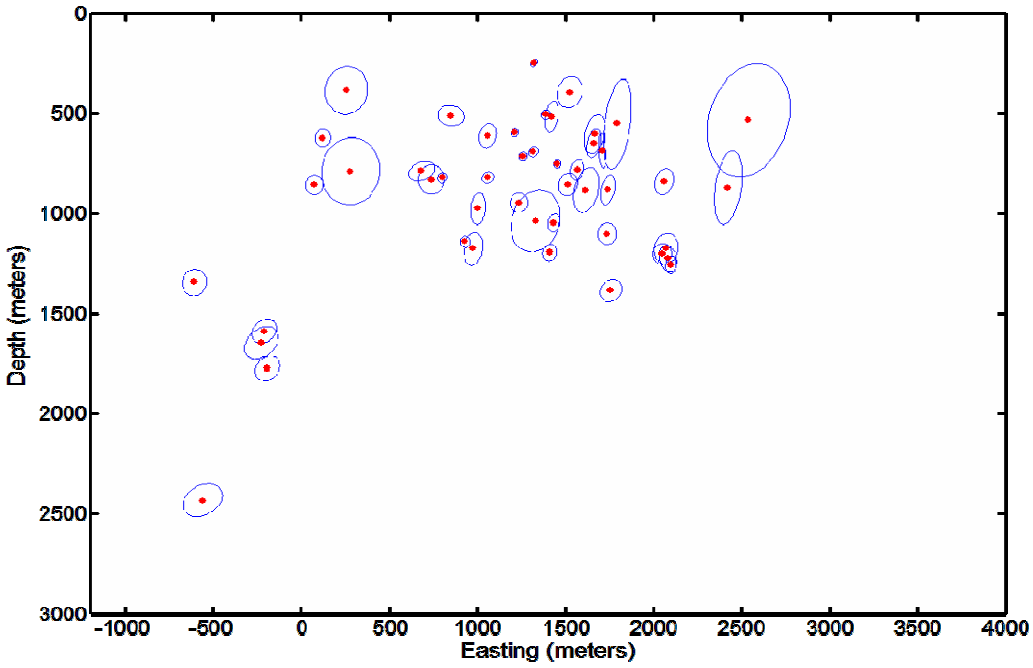

(a)

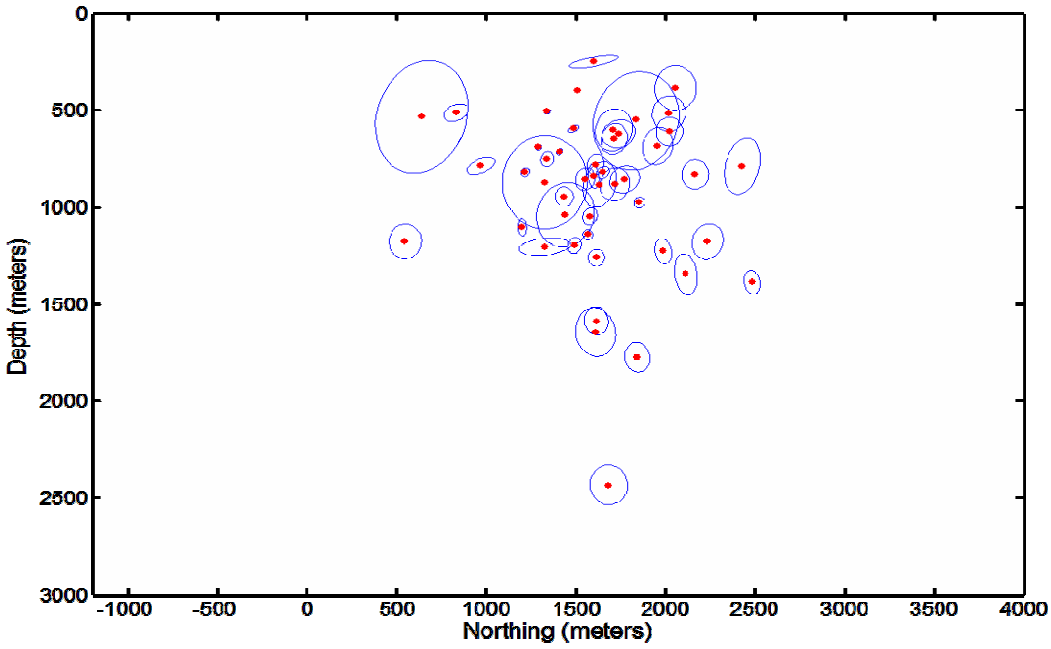

(b)

Figure 6. (a) Vertical (Easting-Depth) distribution of hypocenters (red dots) and corresponding one-standard deviation error ellipses of earthquakes located by the FRANK array. (b) Vertical (Northing-Depth) distribution of the hypocenters (red dots) and the corresponding one-standard deviation error ellipses.

MAGNITUDES

Local magnitudes are generally measured from the peak amplitudes recorded by broadband seismometers at a standard distance from the epicenter of the earthquake. However, the instrumentation of the Turtle Mountain seismic array is band-limited and is ill-suited for magnitude determination. Also, owing to the narrow dynamic range recorded by a single seismometer, it is often impossible to measure the maximum amplitude of strong seismic movements.

Magnitude determination by the duration of a seismic signal is a useful and simple alternative way of measuring the local magnitudes and has been adopted recently at many seismological stations with their own definition of the duration and empirical magnitude formula. Constants applicable to Turtle Mountain were first derived by Bingham (1986) by calibrating the local system (both instrumental and geologic) using published magnitudes of earthquakes between 100 and 700 km. The relationship has the form

$$M_D = -1.93 \pm 0.235 + (2.19 \pm 0.18) \log \tau + (0.00088 \pm 0.00018)\, \Delta \qquad (1)$$

where τ is the duration (s), and Δ is the epicentral distance (km).

In this study, as the coefficient of distance Δ is extremely small and Δs of the local events are less than a few kilometers. For convenience, the distance terms in the formulae are neglected.

Measurement of durations

The duration of a signal, which is often called the *F-P* time, is measured from the first arrival of P-waves to the point where the earthquake signal decays nearly to the ambient background noise level. In this study, measurement of the durations are carried out by using two time windows to acquire both the signal *RMS* amplitude level and noise level previous of the first arrival. Generally, a two-second-long time window is used to get the average ambient background noise level, and a one-second-long running time window starting from the first arrival of P-waves are used to provide the time where the average amplitude level of signal decreases to the average ambient background noise level.

Since the 1986 Turtle Mountain dataset consists of fixed-length event files, many of the microseisms are truncated, making it difficult to measure the *F-P* time directly. To overcome this data limitation, an alternative method of estimating the decay time was developed. Rather than measure the time to decay to the ambient background level RMS_{noise}, we measure the time required to decay to an RMS amplitude greater than the ambient, RMS_{noise}. This level is typically selected to be three times the ambient amplitude. By assuming the dominant frequency of signal and attenuation quality factor Q of the study area, the *F-P* time of the signal is thus estimated.

The formula used to estimate the *F-P* time is based on the relationship

$$A_{RMS}(t)=A_0\exp(-2\pi ft/Q) \quad (2)$$

where $A_{RMS}(t)$ is the *RMS* amplitude at time t; A_0 is the amplitude emitted by the source of an event; f is the dominant frequency of the signals and is assumed to be 15Hz; the quality factor Q is assumed to be 60.

Suppose $A_{RMS1}(t_1)$ is the *RMS* amplitude level which is equal to the pre-existing noise level, and t_1 is time. Similarly, $A_{RMSn}(t_n)$ represents the *RMS* amplitude which is n times higher than the pre-existing noise level. Therefore, the ratio between $A_{RMSn}(t_n)$ and $A_{RMS1}(t_1)$ is expressed by

$$A_{RMSn}(t_n) / A_{RMS1}(t_1) = n = \exp[-(t_n-t_1)\pi f/Q]. \quad (3)$$

By rearranging the formula, the expected *F-P* time t_1 is derived as

$$t_1=t_n+Q\ln(n)/\pi f. \quad (4)$$

After the obtaining the event duration using this relationship, we go on to calculate the event magnitude. To increase the accuracy of the result, the decay time is measured at several stations and averaged. In this study, as all the durations of the locatable events are measurable by at least one of the stations of the FRANK array, we took the average of magnitudes derived from the stations of the FRANK array.

RESULTS

After the magnitudes are measured, we merged the 121 well-located hypocenters determined by the network or the FRANK array, and compared them with the local topography, tectonic weaknesses and geological structures. Detailed information on the events such as event codes, times of origin, locations of hypocenters and numbers of P and S phases used in the hypocenter locating processes is summarized in the Appendix (Tables 1A and 2A).

COMPARISON OF HYPOCENTER DISTRIBUTION WITH TOPOGRAPHY AND TECTONIC WEAKNESSES

To find the distribution features of the events, we plotted the local topography including the extent of debris of the Frank Slide, and the major tectonic weaknesses (major faults and the remaining coal mining) in the study area. The major tectonic weaknesses adjacent to Turtle Mountain are the Turtle Mountain Thrust, remaining coal mining and circular fractures along the western edge of the Frank Slide or close to the peaks (see Figure 7). The NNW-SSE striking Turtle Mountain Thrust can be traced 18 km North and at least 50 km South (Norris, 1955), and it splays into two thrust faults denoted Fault1 and Fault2 in the study area (Map1829A, 1993). The fault planes of the splays of the thrust dip towards west, and the dipping angles are generally regarded to be about 45º (Langenberg, personal communication). The general strikes of Fault1 and Fault2 are bent in the area between the TMB and TMF stations. The general strikes of the northern and southern parts of Fault1 are approximately NW 16º and NW 29º respectively. The general strike of Fault2 is relatively stable, and is approximately NW 23º.

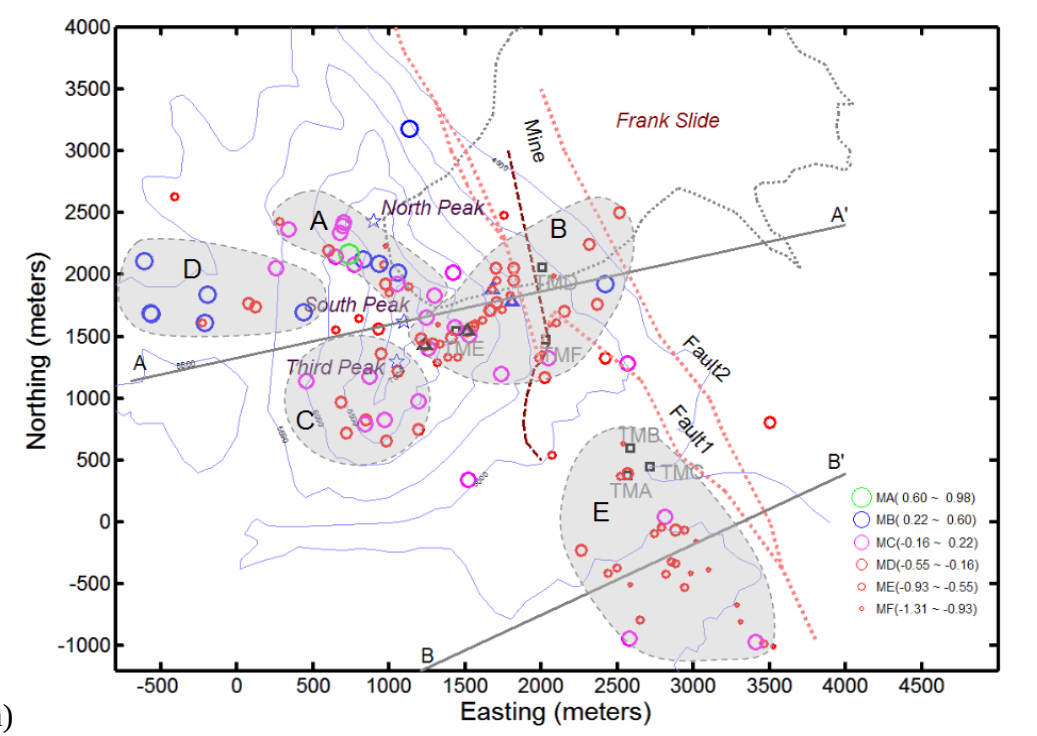

(a)

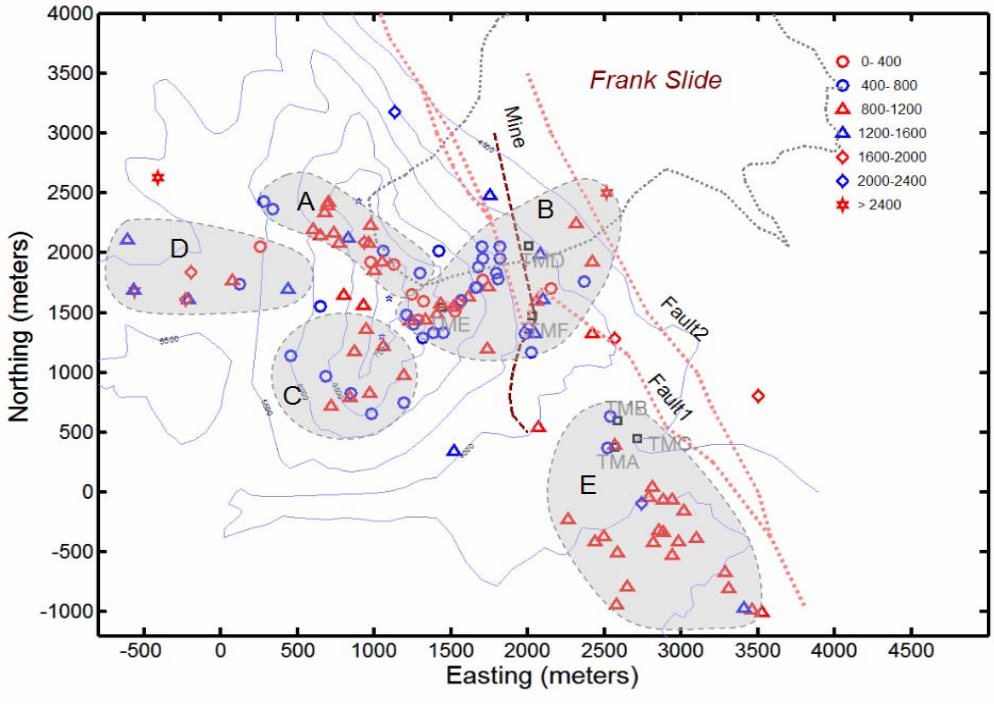

(b)

Figure 7. (a) Lateral distribution of the well-located events and the corresponding *F-P* duration magnitudes. The sizes of the epicenter symbols are scaled according to the six magnitude categories in the legend where magnitude ranges are shown in parentheses. Lines A-A' and B-B' define the profile lines for the depth cross-sections. (b) Lateral distribution of events shown with depths. Depth ranges of events are indicated by symbols in the legend.

For convenience, the range of the duration magnitudes of the microseismic events detected is divided into six relative categories from the minimum MF to the maximum MA. The corresponding ranges of the absolute magnitudes are shown in the key of Figure 7. Laterally, the 121 well-located events mainly concentrate in five areas, denoted by "A" to "E". Events distributing in "A" area occurred between the Third Peak and the South Peak of Turtle Mountain, and trending in a NW-SE direction. The depths of the events in this area range from the surface to approximately 1600 meters. Magnitudes of the events distribute from the minimum MF to the maximum MA to southwest of the Third Peak. In the southern part of the "A" area, both shallower (<800m) and deeper (>800m) events exist, whereas no shallower events are detected on the northern part of the area. This appearance maybe caused by the loss of medium, which blocked the direct propagation of the seismic energies to the FRANK seismic array located to the southeast. Compared with the fracture distribution in the above fracture map (Figure 8), it is obvious that most seismic events coincide with the some fractures between the South Peak and the Third Peak.

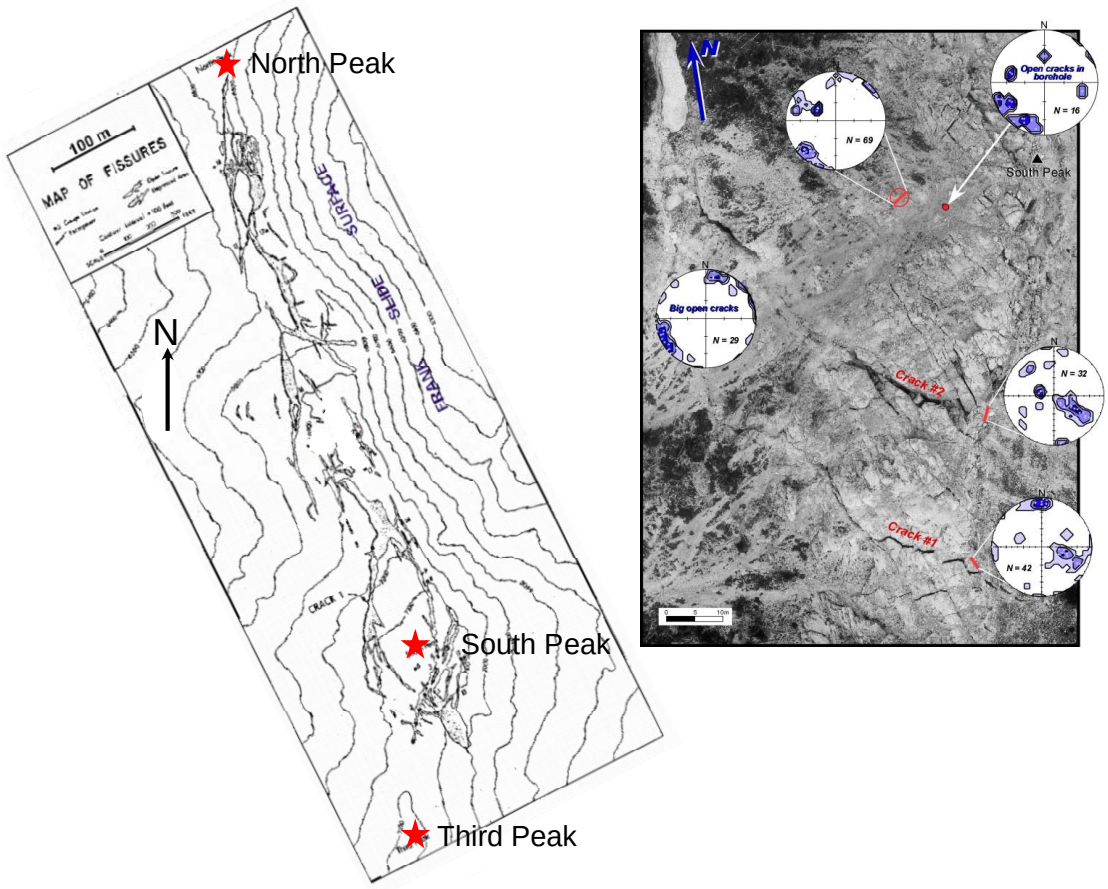

Figure 8. Map of Turtle Mountain fractures (John Allan, 1933). The positions of the three major peaks of Turtle Mountain, North Peak, South Peak and Third Peak are marked by red five-point stars. Major fractures are shaded. (Right) Aerial photo of South Peak with stereonets of fractures and fissures. (Willem Langenberg, 2005).

Close to the southwestern boundary of the Frank Slide (see "B" area), intensive small events (smaller than MC) distribute in NE-SW direction. Most of the events are shallow events close to the surface (less than 800 meters in depth) of the eastern slope of Turtle Mountain (Figure 7b). It should be stressed that both the locations of events and their distribution orientation coincide with the circular fissures there. Such appearance is also observed in the southern part of the "A" area, where many circular fractures also developed. Several events between the TMF and TMD stations occurred very close to former regions of coal mining activity. The cross-sections in Figure 9 through Figure 12 show that such events are located near the surface of the eastern slope. As the coal mining activity was approximately 100 meters below from the surface (Fossey, 1986), it is possible that they originate from the collapse of the mine works.

Events in the "C" area occurred beneath the southern slope of Turtle Mountain are mostly shallow ones from several hundreds meter to 1200 meters in depth. Magnitudes in the area range from MD to MC. Events smaller than MD are not detected in this area by the network although further distant events with magnitude smaller than MD are detected and located in the other areas.

Several deeper events (more than 1400 meters in depth) occurred beneath the western slope of Turtle Mountain in the "D" area. The magnitudes of these events are all of the comparatively larger scale of MB. The distribution of these events shows a trend of dipping towards west. The westward trend increases when they are viewed with the shallow events on the eastern part of Profile A-A' together. It seems that these events, and many of the shallow events distribute along the fault plane of Fault1.

It is interesting that there exists an "aseismic" gap between "E" area and other four mentioned seismic "areas", which is about 800 meters away from the nearest "B" area. Events occurred in "E" area are restricted to the south of FARM array and the west of thrust faults on the ground. The magnitudes of these events range from the smallest MF to the moderate MC, with depths scattering from just below surface to the deepest one of 3000 meters.

CROSS-SECTIONS OF HYPOCENTER DISTRIBUTION WITH GEOLOGICAL STRUCTURES

The major geological structures of Turtle Mountain are Turtle Mountain Anticline and Hillcrest Syncline downward against the Turtle Mountain Thrust. As the dipping angles of the thrusts are unclear, they are assumed to be 45º towards west in this study. The Turtle Mountain Anticline is nearly an upright symmetrical fold with fold axes close to 10-190° in orientation, and the underlying Hillcrest Syncline is an upright asymmetrical fold with fold axes close to 180° (Fossey, 1986). In the study area, the fold axis of both the anticline and the syncline and the strike of the thrusts are slightly close to NNW-SSE direction. Strata in the study area range from the Devonian limestones/interbed dolomites in the core of the anticline to Cretaceous Blairmore Group consisting of sandstones and sandy shales in the core of syncline. Based on the lithologic properties, we divided the strata into three units from old to new. That is, the Paleozoic limestones/interbed dolomites, Jurassic shales, and Cretacious sandstones/interbed sandy shales.

The relationships between the hypocenter distribution and geological structures are illustrated by using two depth cross-sections. The locations of the depth cross-sections are chosen perpendicular to the local structural outlines, where the northern A-A' profile passes through the South Peak and the southern B-B' profile is located about 2.5 km to the south (Figure 7a).

Figure 9 through Figure 12 show the vertical distribution of the events occurred along the A-A' profile within a wide range of 1500m, a narrower range of 500 m on both sides, and in the range of 200m-1500m north or south. Figure 9 shows seismicity activity concentrated along the boundary of anticline and syncline, especially within the hanging wall of Fault1. Magnitudes of events tend to increase with depth, where two events in the scale MB occurred at a depth of 1000 meters. This trend is more obvious in Figure 9. Most events occurred in the area "A" show to be a cluster just above the fault plane of Fault1. Along the axes of syncline or within the hanging wall of Fault2, scattered seismic activity also exists.

The vertical distribution of the seismic events in area "B" are highlighted in the cross-section (Figure 9, Figure 10). In that region most events occurred beneath the surface of the eastern slope of Turtle Mountain at depths less than 800 meters. This depth range is approximately extends from the peak of Turtle Mountain to its base. Although the depth of the fractures in this area is unclear, the length of the large fractures at surface is estimated in the order of 100 meters (Spratt and Lamb, 2005). The width of one of the largest fractures (Crack #1) is as wide as approximately 1 meter at the top (Theune et al., 2005). Thus, it is possible that the fissures extended as deep as 800 meters, and the seismic events occurred throughout the depths.

The depths of the microearthquakes located below the southern slope of the "C" area are pinpointed in Figure 11. Clearly, most of the events in the "C" area occurred in the Paleozoic limestone/interbed dolomites layer of the Turtle Mountain Syncline.

The comparatively large magnitude events in "D" mainly occurred in the deep parts of the Paleozoic limestone layers. It is interesting that these events along the fault plane or within the hanging wall of the Fault1 viewing from the cross-section A-A'.

The relationships between the distribution of the events and the local geological structures in the area "E" is shown in Figure 12. In that figure, hypocenters within the range of 1000 meters on both sides along the profile B-B' are projected onto the section. We see events located adjacent to the axes of Turtle Mountain Syncline ranging from approximately 200 m to 600m below the ground. This is similar to what we see in cross-section A-A'. There are more seismic events close to the fault planes in the eastern limb of the syncline in the similar depths. The magnitudes of the events are smaller than MC.

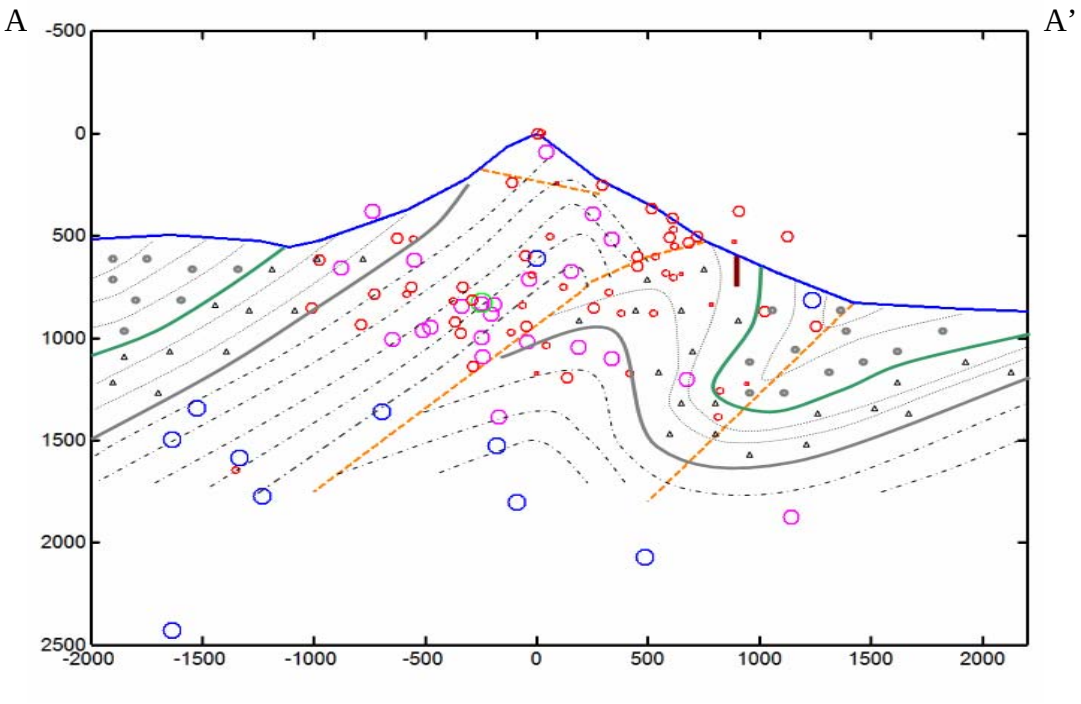

Figure 9. Cross-section along Profile A-A' from Figure 7a. Hypocentres within 1500 m of A-A' have been projected onto the section.

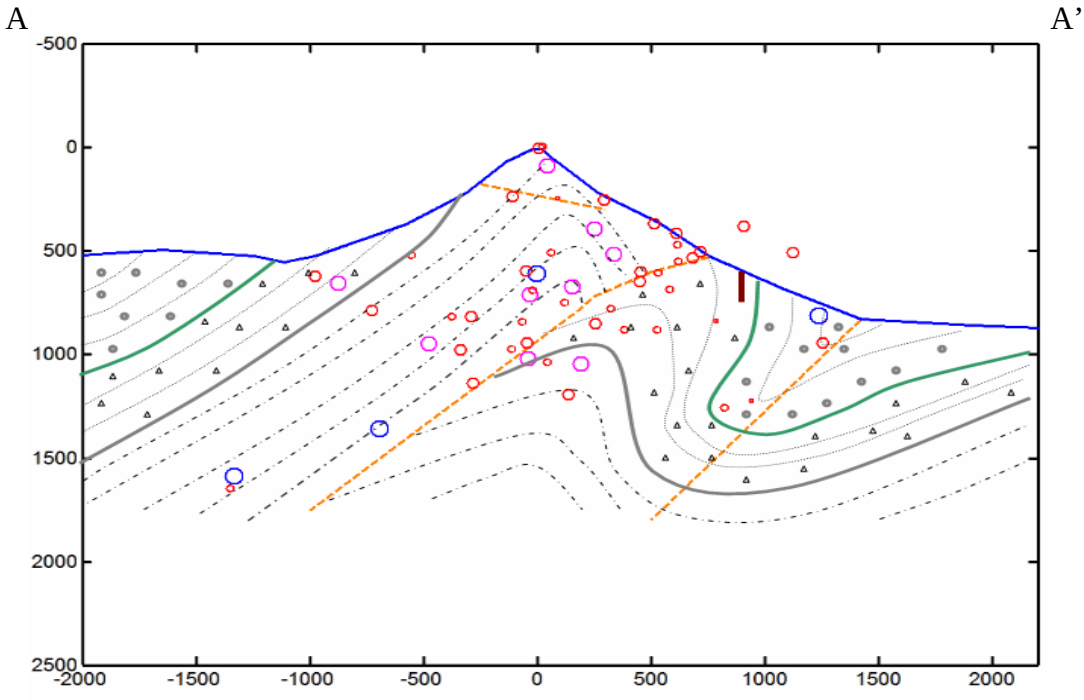

Figure 10. Cross-section along Profile A-A' showing hypocentres within 500 m of A-A'.

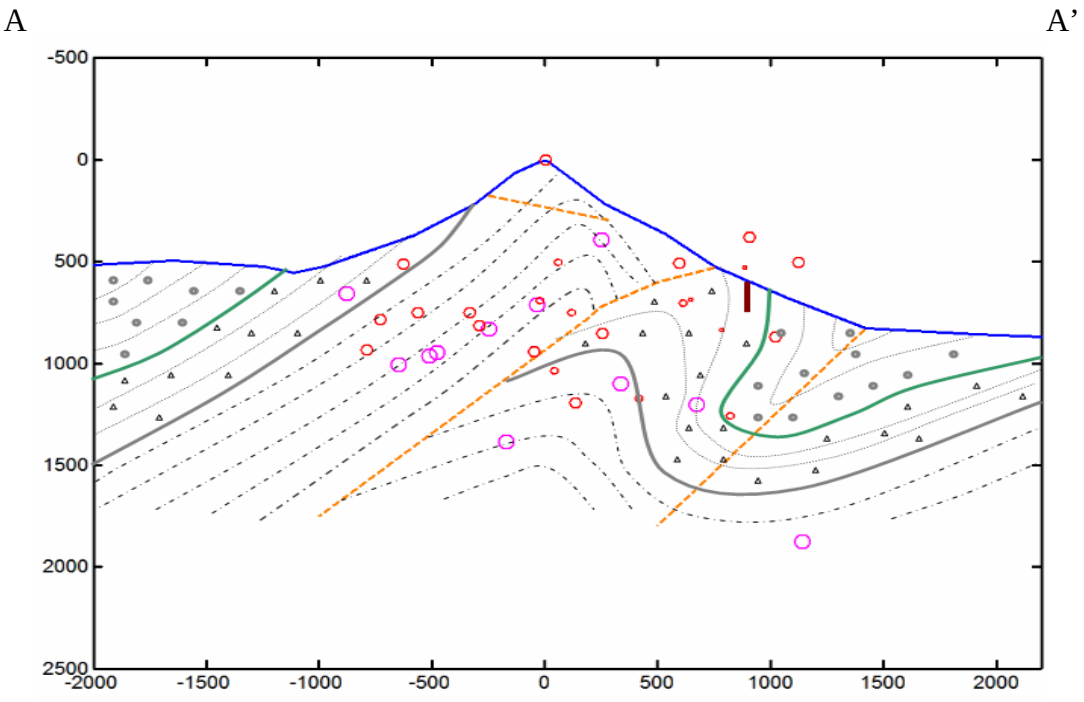

Figure 11. Cross-section along Profile A-A' showing hypocentres within 200 m to 1500 m of A-A'.

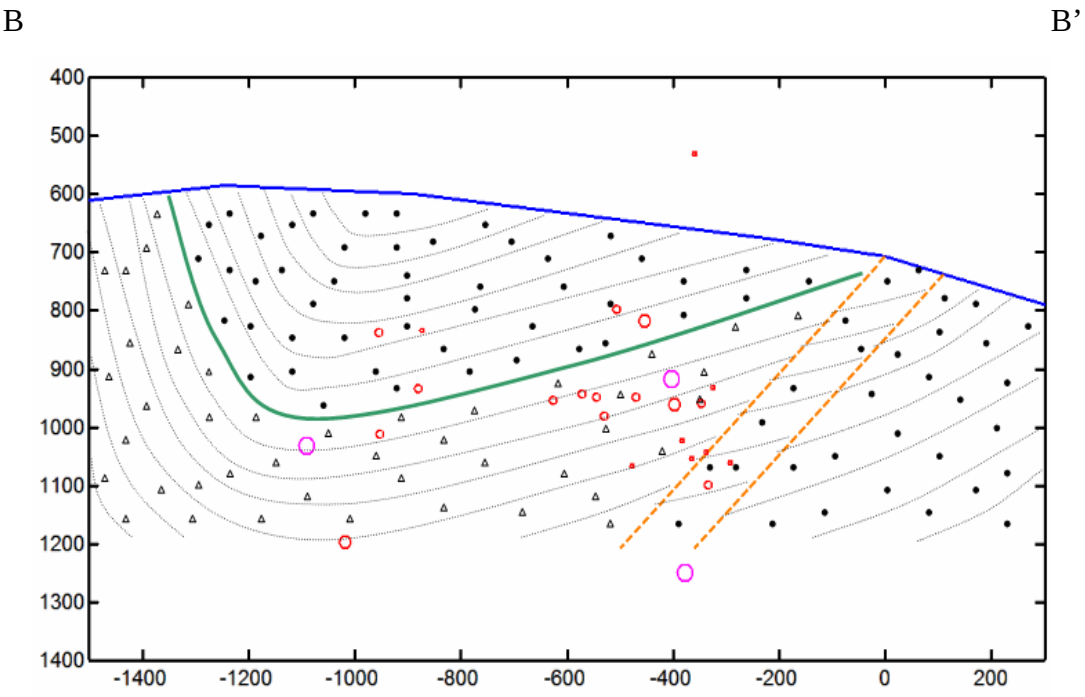

Figure 12. Cross-section along profile B-B'. Hypocentres within 1000 m of B-B' have been projected onto the section.

DOUBLE MICROEARTHQUAKES

Several double microearthquakes have occurred adjacent to the TMD station during the period of observation. The time intervals between the two sub-events range from less than 1 to 10 seconds. Two of such events have been located by the network (see the events highlighted in Tables 1A and 2A). Although the two sub-events are not located to the same focus due to the limited configuration and number of stations, the similarities of waveforms recorded by different stations strongly suggest that their sources are very close each other. In spite of the location errors, the results indicate us that these unique events happened very close to the southwestern rim of the Frank Slide.

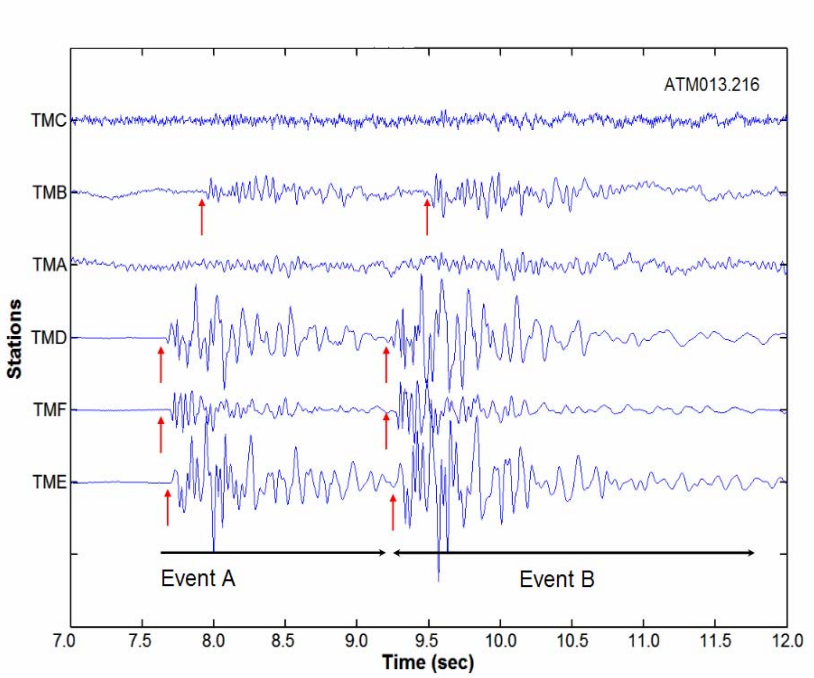

Figure 13. Example seismograms of a double-microearthquake recorded in April, 1991 by the seismic network. Stations codes are shown at the beginning of each recording; The first arrival of the two individual sub-events in each station is indicated by a red arrow. The first arrivals in TMA and TMC stations are not identified.

EARTHQUAKE SWARMS

Five earthquake swarms have been detected by the seismic network in the eastern vicinity of Turtle Mountain. These events appear as clusters with nearly identical waveforms, magnitudes and occurred within short time periods. Weichert and Horner (1981) reported three localized swarms of microseisms occurring from June to September, 1981.

Of the five earthquake swarms observed by this study, four of them are characterized with distinct first arrival times of P and S-waves by at least three stations, and thus are locatable (Table 2).

The occurrence of the swarms ranges from the end of 1987 to the beginning of 1989. Swarm 1 is divided into two stages of 44 and 88 minutes with a pause time of nearly 8

days. The durations of Swarms 2 and 3 are 87 and 43 minutes respectively; Swarm 4 occurred in two stages with a pause of about 10 hours; Swarm 5 is also divided into two stages, and the shows a pause time of nearly 3 days. Note swarms with time durations of a few hours have been reported elsewhere by (Frémont and Malone, 1987). The number of events of each microseismic swarm ranges from 10 to 19.

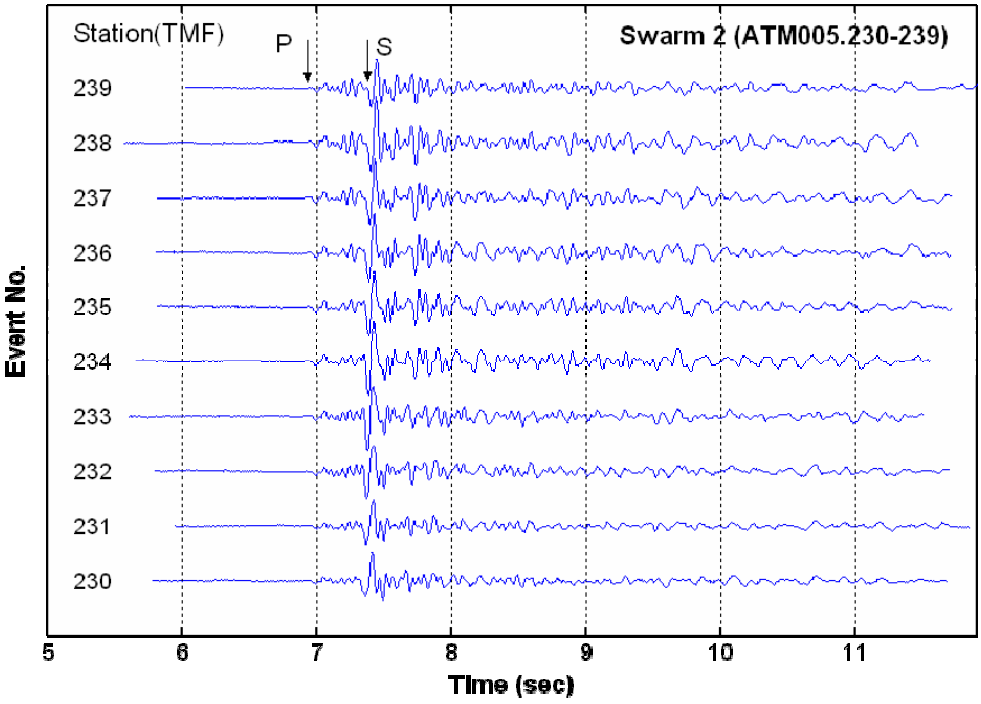

Figure 14. Example seismograms of ten microseisms of Swarm 2 recorded at TMF station. Plotting ranges of seismograms are adjusted to make the positions of P, S-waves easier to compare from trace to trace.

Table 2. Event codes, start times, ending times, durations and event numbers of the five swarms detected during the period of observation. Swarm 1, 4 and 5 are divided into two stages with pause times of eight days, ten hours and three days respectively.

Swarm#	Event code	Start time				Ending time				Duration (min)	Total events
		yy	dd	hh	mm	yy	dd	hh	mm		
Swarm1 *	ATM003.337-340	1987	257	17	11	1987	257	17	55	44	9
	ATM350-355 (no 354)	1987	265	18	16	1987	265	19	40	84	
Swarm2 +	ATM005.215-224	1988	323	21	51	1988	323	23	18	87	10
Swarm3 +	ATM005.230-239	1988	325	12	18	1988	325	13	01	43	10
Swarm4 +	ATM005.247-255	1988	327	04	15	1988	327	05	51	96	16
	ATM005.259-265	1988	328	16	27	1988	328	17	11	44	
Swarm5 x	ATM006.136-153 (no 138,140,148)	1989	035	02	06	1989	035	09	45	459	19
	006.168-171	1989	038	05	09	1989	038	10	01	292	

Symbols *, +, x represent the swarm located by the whole network, FRANK array, and not located respectively.

Locations of hypocenters from Swarms 1 to 5 are shown in Figure 15 and Figure 16. The hypocenters of Swarm 1 are well located and concentrate below the middle southern boundary of the Frank Slide debris. Depths of these events range between 1.5 and 2.0 km, which is approximately 700-1200 km below surface. The hypocenter locations of the Swarm 2 are less accurate and scatter below the southeastern boundary of the slide debris. All the events except one in Swarm 3 are located in a small lateral space of 300m x 500m. This swarm occurred beneath the southeastern boundary of the Frank Slide debris. Further, most hypocenter depths are 2000 to 2500 meters in depth. The sixteen events of Swarm 4 are located below the eastern part of the Frank Slide debris. Similar to the previous swarms, the depths ranges from 1300 to 2500 meters in depth. Because the first arrival times of Swarm 5 are not clearly recorded by more than three stations, the locations of the events are not locatable.

Microseism swarms occurred about 1-3 km northeast of the FRANK array or 2-4 km northeast of the peaks of Turtle Mountain. In depth, they lie approximately 0.5-2.0 km beneath the Frank Slide debris.

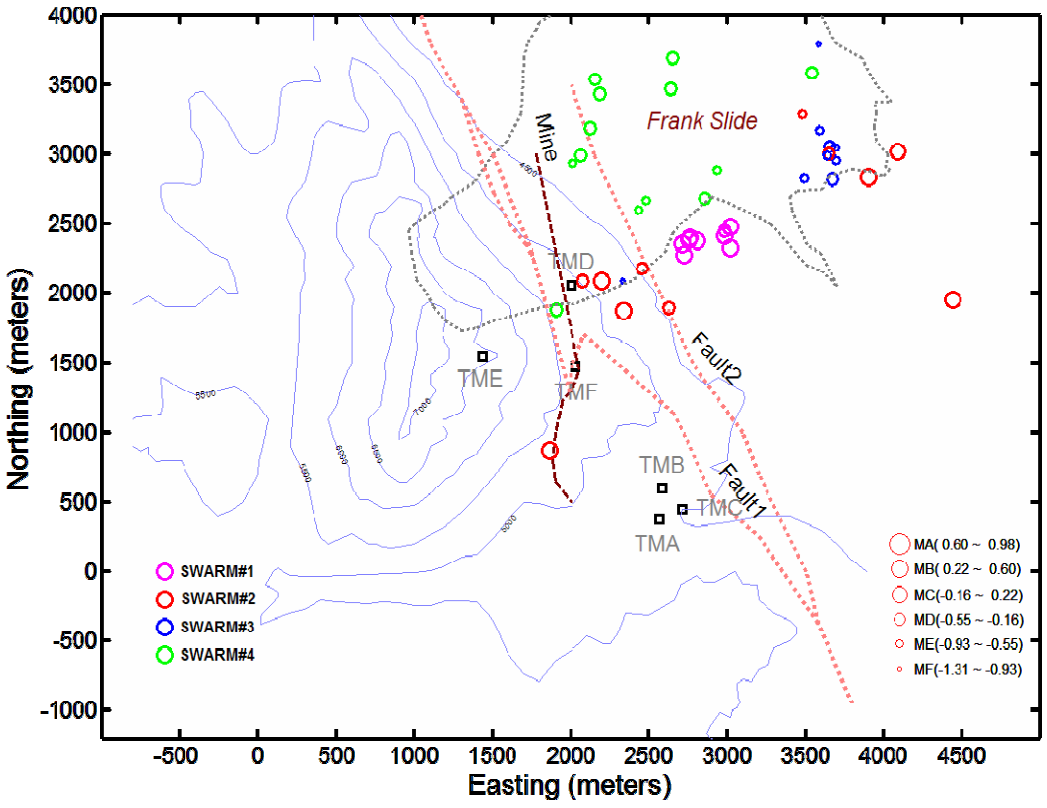

(a)

Figure 15. Lateral distribution of the seismic swarms by the network.

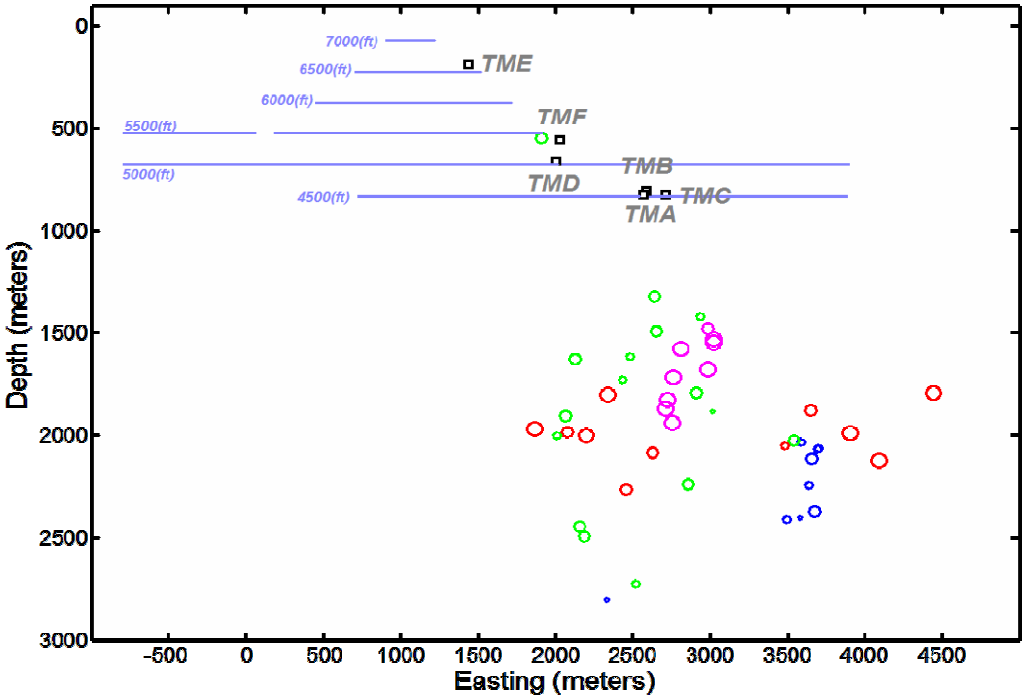

Figure 16. Vertical distribution of the seismic swarms recorded by the network.

FOCAL MECHANISMS

The local seismic array, which is composed of only six observation stations and deployed closely together, makes it difficult to determine the focal mechanisms of events. Further, the magnitudes ($M_{F\text{-}P}$) of most microearthquakes located are too small to be recorded by the nearby regional observation network. We thus attempted to detect the upwards or downwards directions of the first-motions of the P-waves of the events recorded by our local arrays, and find out or exclude some possible focal mechanisms.

When a P-wave reaches a vertical geophone, the first motion will be either upgoing or downgoing, based on the polarity of the initial displacement. For each microseismic event, we can collect the set of polarities as recorded at each monitoring station. At Turtle Mountain, the polarity sets are not random – there are certain polarity patterns which are more common than others. The six most common found polarity patterns are shown in Figure 18a. The two most common are “all upwards” and “all downward”. We shall call these patterns type #1 and type #2 respectively. As the number of the observation stations is limited and the configuration of the array is narrow, there could be several focal mechanism which result in the same pattern.

In Figure 17, events with pattern-type #1 (all-upwards) are concentrated in two shaded rectangular zones with their major axis parallel to the Turtle Mountain Thrust. We may use the direction of first motion to help determine the nature of the NNW-SSE fractures/ruptures. The direction of first motion produced by double-couple sources can be predicted according to the geometry of the stations relative to the microseism hypocentres. The observed first arrival polarities best match the case where the NNW-fractures are of a dip-slip (thrust) nature, rather than a strike-slip nature.

In the area between the shaded zones, almost all the events are of pattern type #2 (all-downwards). To interpret this, we refer to the schematic diagram (Figure 18b), where the relationships of the fault planes and the observation stations, stress-field orientation and first motions are illustrated. From the diagram, we see that an observation station located either on the eastern side of the horizontal fault projection, or on the western side of the auxiliary fault projection generates an upward motion. Similarly, if the observation station is located between the two horizontal projections, the first motion will be downwards.

First motion patterns types #3-#6 mainly exist adjacent to the peaks of Turtle Mountain and the southwestern edge of the Frank Slide. Here, local small-scale normal faults and widely-spread fractures exist. The microseisms are likely caused by the slip of these fractures.

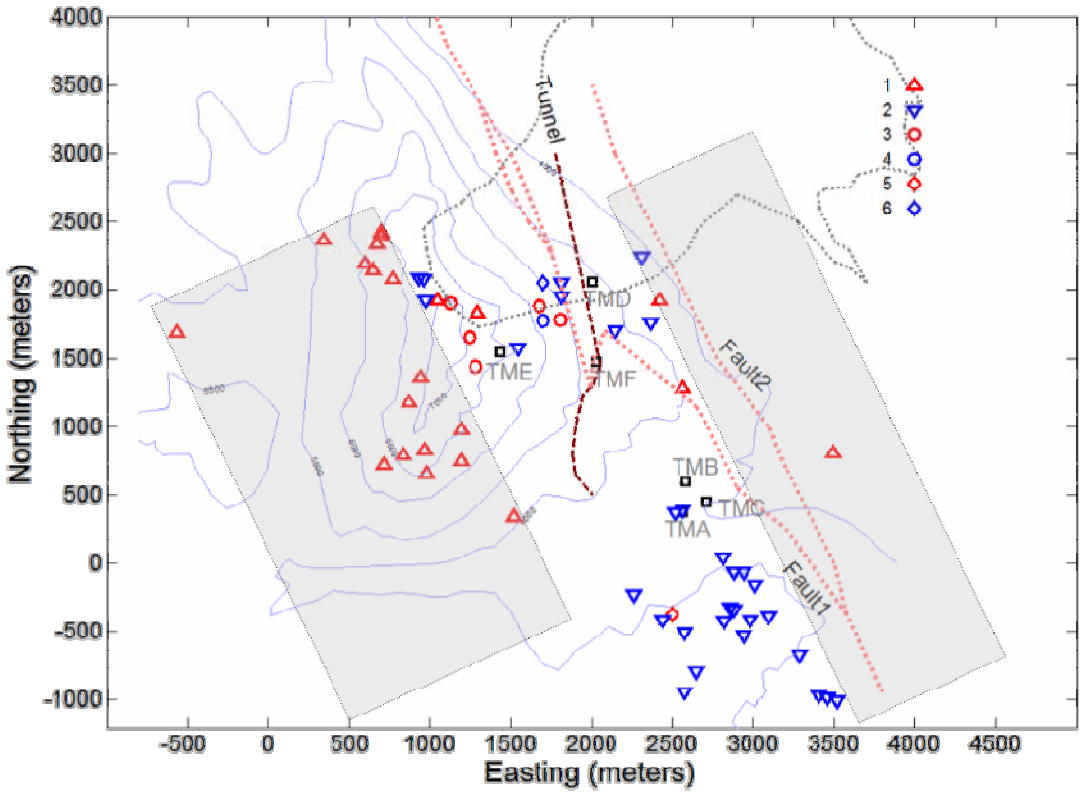

Figure 17. Lateral distribution of the events with distinguishable P-wave first motions on the recordings of the six network stations. The key in the upper right corner indicates the types of patterns of first motions.

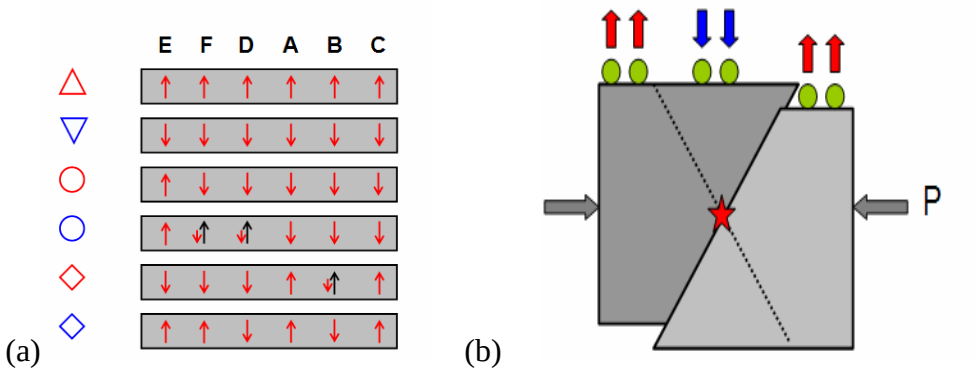

Figure 18. (a) Patterns of P-wave first motions on the seismograms recorded by six network stations. The stations TME,TMF, TMD,TMA,TMB and TMC are designated by letters E, F, D, A, B and C respectively. Red Arrows indicate the directions of first motions. In Pattern #3-#4, the weak first motions (short red arrows) are replaced by the reverse strong first motion (black arrows) immediately; (b) Illustration of the relationships between the direction of the first motion of geophones and the maximum compressive principal stress (P), as a function of station locations and lateral projections of a thrust fault plane and its auxiliary. The source of an earthquake is represented by a five-point star. Geophones locations are represented by circles and first motion of geophones is indicated by solid arrows.

DISCUSSION

In this study, the existence of local microseismic activity within Turtle Mountain and the surrounding area is confirmed. Based on the comparison between the distribution of the seismic events and topography, tectonic weaknesses, geological structures and focal mechanisms of sources, it seems that the origins of the microseisms are related to movement along the local tectonic weaknesses.

One important purpose of deploying the seismic network was to monitor microseismic activity near the abandoned coal mine works. The mine has always been considered the trigger of the Frank Slide as it presumably weakened the support of the overlying rocks. We would expect to observe some intensive seismic activity close to the coal tunnels; however, few events lie along it. The absence of present-day seismicity along the coal mine casts some doubt on whether collapse of the coal mine caused the 1903 landslide.

The anticlinal structures with steeply-dipping bedding planes, and the circular-shaped fractures on the mountain top, has been considered as another cause of the landslide. It is interesting that areas of intense seismic activity (areas “A” and “B”) coincide with the southern part of the circular fractures. A variety of focal mechanisms in this area also suggests the existence of fracture movements different from the local major NNW-SSE strike of the tectonic weakness. Based on the evidence, it is likely that these circular fractures adjacent to the landslide are active, and are the source of the local microseismic activities. As mentioned before, the lack of shallow seismic events in the northern part of area “A” may be caused by the loss of medium. Due to the air gap, the seismic energy is unable to propagate to the observation array on the other side of the landslide. Similarly, shallow events occurred along the northern circular fractures, would also go undetected by the FRANK array. This explains the lack of microseismicity detected along the

northern part of the circular fractures. If this theory is true, then the whole the circular fractures encircling the rupture surface of the Frank Slide between the South Peak and the Third Peak could still be active. Monitoring of the whole circular fracture between the North Peak and the Third Peak is recommended as it may ultimately provide notice of a future landslide.

Based on the observation and results, we try to explain the cause of the Frank landslide.

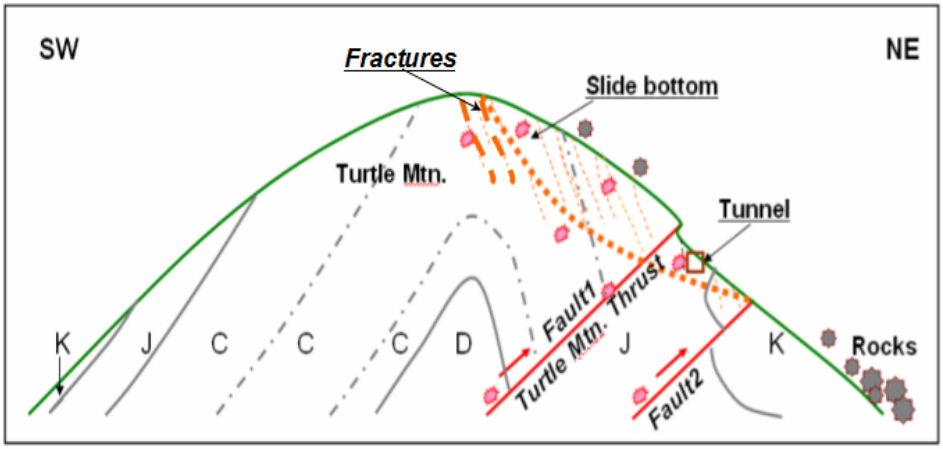

Figure 19. Schematic SW-NE cross section of Turtle Mountain and Frank Slide showing the mechanisms of microseisms at Turtle Mountain. The cross section is suppose passing across the peak of Turtle Mountain and perpendicular to contour lines on the northeast slope of the mountain. Positions of thrust faults (solid red lines with arrows), mine tunnel (square), bottom of slide body (bold dotted line), fractures (dotted lines) and hypocentres of related possible microseisms (explosions) are also shown. Boundaries between strata are indicated by solid or dot-dashed lines.

Before the landslide, eastward movement of the hanging wall of the thrust Fault1 weakened or lost the support overlying loads and led to rock fractures, rock falls, microseisms, and caused a weakened geological body full of fractures. If this is true the general strike of the induced fractures should be parallel to that of the thrust faults and have steep dipping angles. Geological surveys support this prediction (e.g. Allan's fissure map, 1933; Spratt and Lamb, 2005). The landslide occurred along the bottom of the weakened geological body or some large fractures when the overlying loads surpassed some supporting limitation. This viewpoint matches the theory of the collapse of the anticlinal geological structures with steeply dipping bedding planes at the eastern slope of Turtle Mountain.

After the landslide, similar tectonic processes continue along the Fault1 and its adjacent regions. The movements of the fractures at present are supported by the microearthquakes detected during this observation. The fact that the rock slide falls only on the eastern slope of the mountain observed by local people (Bingham, 1996) also support the idea.

The other speculated causes of the landslide such as the collapse of the coal mining at the eastern foot of Turtle Mountain, heavy rains and frost just before the landslide, major

earthquake tremor in 1901 could be interpreted as the factors that stimulated and accelerated the movement of induced fractures adjacent to the top of Turtle Mountain.

On a broader scale, rock slides commonly occur in the southern Canadian Rocky Mountain especially on their eastern flanks (Cruden, 1986). Jones (1993) has mapped an ancient major rock slide below Bluff Mountain immediately to the north of Turtle Mountain with its scale about 10 times larger than Frank Slide in Turtle Mountain. As thrust faults with N-S strikes develop extensively beneath the Rocky Mountain and are exposed on the eastern flanks, the processes of such faults and the accompanying rock fractures within the hanging walls may be related to the rock slides.

CONCLUSIONS

Based on the above results and discussion, the following conclusions on the microseismicity at Turtle Mountain are drawn:

1. The existence of the local microseismic activity at Turtle Mountain and its vicinities is confirmed. The magnitudes of events are smaller than $M_{F\text{-}P}1$. This indicates that only extremely small seismic activity exists. The depths of the events range from surface to approximate 3.0 km from the top of Turtle Mountain.

2. The distribution of the microseisms may be related to weaknesses such as surface fractures, coal mining remnants, and fault planes of the Turtle Mountain Thrust. The most intensive seismic areas occurred on the eastern slope of Turtle Mountain.

3. Some spatial correlation of the intensive shallow seismic areas with the circular fractures between the South Peak and the North Peak suggests that the fractures may be active.

4. Several events coincide with the remaining coal mining region. It is still difficult to affirm that they are attached to the collapse of the mined volumes.

5. Shallower events (less than 0.5 km from surface) do not seem to occur within the Frank Slide debris. However, microseismic swarms occurred frequently below the east and southeastern boundary of the Frank Slide. The depth is approximately 0.5-1.5 km below the surface.

ACKNOWLEDGEMENTS

We would like to thank Dr. D. Bingham for providing the seismic data in this study. We would also thank Professor N. Hirata of ERI of the University of Tokyo, Japan for providing us the computer program HYPOMH. We also thank Dr. Rolf Maier and Kevin Hall of CREWES project for their helpful comments on this paper.

REFERENCES

Allan, J.A., 1931, Report on Stability of Turtle Mountain, Crowsnest District, Alberta: Dept. of Public Works, Edmonton: Alberta Provincial Archives.

Bingham, D.K., 1996, Seismic monitoring of Turtle Mountain: Internal report, Alberta Environmental Protection, Government of Alberta.

Bland, H.C., Stewart R.R., Bertram M.B., Gallant E.V. and Thurston J., 2003, A remote, wireless microseismic monitoring system: CREWES Research Report, **6**.

Cruden, D.M., 1986, Monitoring the south peak of Turtle Mountain, 1980-1985: RMD Report 86/37, Alberta Environment, Edmonton, 59pp.

Fossy, K.W., Structual geology and slope stability of the southeast slope of Turtle Mountain, Alberta: master's degree thesis, University of Alberta, 1986.

Frémont, M.J., Malone,S.D., 1987, High precision relative locations of earthquakes at Mount St.Helens, Washington: J.Geophys.Res., **92**, 10,223-10,236.

Jones, P.B., 1993, Structural geology of the modern Frank slide and ancient Bluff Mountain Slide, Crowsnest, Alberta: Bull. Can. Petro.Geol., **41**, 232-243.

Map 1829A, 1993, Geology and structure cross-sections, Blairmore (West Half), Alberta, Scale 1:50000: Geological Survey of Canada.

McConnell, R. G., and Brock R.W., 1904, Report on the great landslide at Frank, Alberta, Canada: Canadian Department of the Interior, Annual Report, 1902-1903, part 8, 17p.

Hirata, N., and Matsu'ura, M., 1987, Maximum-likelihood estimation of hypocenter with origin time eliminated using nonlinear inversion technique: Phys. Earth Planet. Inter., **47**, 50–61.

Spratt D. A., and Lamb M.A., 2005, Borehole data interpretation and orientations, Turtle mountain monitoring project: WP15b Report, Department of Geology & Geophysics, University of Calgary, 1-15.

Theune, U., Schmitt, D. and Sacchi M., 2005, Looking inside Turtle Mountain: Mapping fractures with GPR: Recorder of CSEG, **30**, 34-38.

Weichert, D.H., and Horner, R.B., 1981, Microseismic monitoring in Blairmore, Alberta: Internal Report 81-4, Earth Physics Branch, Energy, Mines and Resources Canada, Ottawa, 27pp.

APPENDIX

Table A1. Summary of hypocenters of the microseisms located by the network. The event codes shown in bold, are double-microearthquakes.

Eq.#	Event Code	Time of Origin					Location			Phases used		Magnitude
		year	day	hour	min.	sec.	x(m)	y(m)	z(m)	P	S	(M_{F-P})
1	ATM016.208	1992	212	06	26	11	1981.9	1322.5	702.5	4	4	-0.794
2	ATM016.190	1992	181	16	47	44	2785.8	-42.2	947.9	6	6	-0.682
3	ATM016.098	1992	134	04	43	14	2813.3	46.4	917.8	6	6	-0.013
4	ATM015.304	1992	74	11	36	17	3014.8	-157.0	931.3	6	5	-0.962
5	ATM014.245	1991	281	17	29	03	2563.9	392.8	817.6	6	4	-0.472
6	ATM014.210	1991	259	20	46	36	2003.5	1365.3	685.3	6	5	-1.002
7	ATM014.150	1991	223	17	58	03	3097.1	-386.7	1053.6	5	5	-1.306
8	ATM014.004	1991	150	20	33	42	827.3	2121.7	1524.5	6	6	0.300
9	ATM013.357	1991	150	20	33	42	933.5	2089.8	1804.1	6	4	0.300
10	ATM013.340	1991	142	21	04	27	2262.7	-229.3	1195.9	6	3	-0.510
11	ATM013.330	1991	138	13	21	24	3286.9	-672.0	1043.1	6	4	-1.164
12	ATM013.278	1991	118	09	02	04	2880.0	-60.7	960.7	6	6	-0.456
13	ATM013.252	1991	109	16	53	51	3460.9	-979.2	1098.9	6	6	-0.892
14	ATM013.238	1991	103	15	08	27	1127.7	1901.8	-4.1	6	2	-0.885
15	ATM013.237	1991	103	09	15	15	1702.7	1773.0	367.8	6	4	-0.166
16	ATM013.235	1991	103	07	33	11	2647.5	-791.4	837.6	6	6	-0.672
17	ATM013.233	1991	102	23	22	26	2982.8	-413.9	1066.3	6	6	-0.992
18	ATM013.224	1991	101	09	39	10	2853.0	-318.6	948.8	6	6	-0.816
19	**ATM013.216B**	1991	96	09	14	50	1806.6	1783.9	470.2	6	4	-0.868
20	**ATM013.216A**	1991	96	09	14	48	1678.2	1884.7	603.3	6	4	-0.898
21	ATM013.215	1991	96	08	39	30	1697.7	2051.2	412.4	6	6	-0.278
22	ATM013.175	1991	75	17	35	01	3522.1	-1003.7	1060.3	6	5	-1.092
23	ATM013.113	1991	52	22	31	49	-411.8	2630.0	2734.9	6	2	-0.655

24	ATM013.091	1991	45	06	25	54	2818.8	-423.4	953.8	6	4	-0.565
25	ATM013.090	1991	44	23	00	43	3308.1	-803.8	1022.8	6	5	-1.112
26	ATM013.088	1991	44	14	41	48	977.0	1921.5	237.6	6	6	-0.433
27	ATM012.294	1990	341	21	41	21	2022.8	1167.3	506.2	6	6	-0.481
28	ATM012.251	1990	325	01	16	45	2579.5	-502.1	833.5	6	4	-0.997
29	ATM012.070	1990	258	17	21	42	1519.8	339.6	1384.3	6	5	-0.158
30	ATM012.068	1990	257	22	31	54	1191.4	746.8	750.6	6	2	-0.287
31	ATM012.067	1990	257	22	25	26	980.6	654.4	752.2	6	2	-0.290
32	ATM012.066	1990	257	21	24	43	1193.6	973.1	831.7	6	5	-0.068
33	ATM012.005	1990	225	15	02	15	1815.7	1953.4	532.9	6	2	-0.312
34	ATM012.002	1990	224	07	09	40	2516.7	368.9	798.1	6	2	-0.651
35	ATM011.332	1990	225	15	02	15	1814.6	2052.3	503.0	6	3	-0.312
36	ATM011.329	1990	224	07	09	40	2877.7	-332.5	981.6	5	3	-0.649
37	ATM011.298	1990	208	18	09	21	696.2	2391.9	884.7	6	3	-0.026
38	ATM011.297	1990	208	18	04	36	698.2	2419.5	837.1	6	2	0.077
39	ATM011.296	1990	208	15	32	24	649.9	2145.0	845.9	6	3	-0.066
40	ATM011.295	1990	208	15	29	41	598.1	2197.4	921.1	6	3	-0.177
41	ATM011.287	1990	205	19	25	40	337.0	2368.8	619.4	6	2	-0.106
42	ATM011.286	1990	205	19	17	21	767.6	2082.9	999.3	6	3	-0.028
43	ATM011.285	1990	205	19	13	48	673.9	2340.5	1092.1	6	2	-0.103
44	ATM011.245	1990	200	17	59	28	967.3	829.4	964.4	6	4	0.142
45	ATM011.243	1990	200	17	19	55	838.3	788.2	1007.6	6	6	-0.006
46	ATM011.242	1990	200	17	16	29	714.4	719.3	933.4	6	5	-0.216
47	ATM011.187	1990	166	11	14	41	3403.1	-969.9	1250.2	6	4	0.189
48	ATM011.156	1990	157	07	36	44	2439.0	-411.4	1012.4	6	4	-0.759
49	ATM011.143	1990	152	18	31	56	2939.8	-63.9	958.7	6	5	-0.808
50	ATM011.131	1990	148	12	42	30	2738.2	-91.6	2194.5	6	3	-0.782
51	ATM011.075	1990	131	20	46	30	438.5	1694.7	1358.7	6	1	0.303
52	ATM011.052	1990	123	23	29	35	2314.3	2245.3	941.8	6	1	-0.474
53	ATM011.038	1990	120	23	28	08	2496.3	-367.2	934.0	6	4	-0.905
54	ATM011.033	1990	118	18	47	25	2575.5	-941.0	1030.9	5	3	-0.077
55	ATM010.317	1990	99	02	15	30	644.9	1550.5	518.5	5	3	-0.844
56	ATM010.257	1990	81	02	45	38	2150.2	1701.4	378.7	5	3	-0.201
57	ATM010.175	1990	61	16	12	48	456.3	1143.3	655.3	5	2	0.072
58	ATM007.216	1989	202	12	31	08	-569.7	1691.5	1496.2	5	2	0.500
59	ATM007.149	1989	162	21	41	40	2363.3	1757.3	505.1	6	3	-0.255
60	ATM007.113	1989	152	12	01	26	1284.8	1437.9	2.7	6	0	-0.205
61	ATM007.008	1989	100	21	53	40	1545.1	1572.1	250.9	4	4	-0.383
62	ATM006.315	1989	75	15	56	43	2938.9	-528.7	943.3	6	4	-0.841
63	ATM006.092	1989	25	12	17	16	1244.1	1651.8	89.1	5	1	-0.054
64	ATM006.073	1989	22	19	17	32	964.7	2079.3	841.6	4	3	-0.780
65	ATM004.333	1988	222	00	07	52	2418.7	1924.9	813.0	5	4	0.294
66	ATM004.243	1988	131	23	41	51	1134.4	3175.4	2069.3	5	4	0.247
67	ATM004.210	1988	117	15	03	41	1293.2	1829.4	673.6	4	2	0.199
68	ATM003.359	1987	266	16	11	58	946.8	1362.5	975.8	6	5	-0.187
69	ATM003.358	1987	266	14	20	17	870.5	1177.3	946.1	6	4	-0.094
70	ATM003.344	1987	259	15	00	13	1048.4	1924.0	1017.4	6	4	0.203
71	ATM003.056	1987	136	22	46	54	2055.4	1924.1	2910.4	4	4	-0.835
72	ATM003.151	1987	155	14	03	45	2534.8	1285.1	1876.1	5	4	0.003
73	ATM003.187	1987	169	16	09	07	3499.1	803.8	1962.4	5	2	-0.402

Table A2. Summary of hypocenters of the microseisms located by the FRANK array. The events codes shown in bold are the double-microearthquakes.

Eq.#	Event Code	Time of Origin					Location			Phases used		Magnitude ($M_{F\text{-}P}$)
		year	day	hour	min.	sec.	x(m)	y(m)	z(m)	P	S	
1	ATM018.133	1995	158	06	14	36	845.9	829.2	511.2	3	3	-0.413
2	ATM018.132	1995	158	02	30	14	120.0	1736.5	620.9	3	3	-0.322
3	ATM018.131	1995	158	01	58	07	253.4	2053.9	381.8	3	3	-0.131
4	ATM018.130	1995	158	01	44	34	72.4	1769.3	853.5	3	3	-0.220
5	ATM018.129	1995	158	00	26	39	-229.8	1608.0	1644.4	3	3	-0.747
6	ATM018.114	1995	133	18	46	14	2079.5	1985.2	1223.7	3	2	-1.250
7	ATM017.212	1994	10	07	16	52	680.6	966.9	784.4	3	2	-0.339
8	ATM016.234	1992	240	12	28	41	1522.2	1509.8	392.3	3	3	-0.108
9	ATM006.111	1992	139	23	28	12	1318.2	1597.1	245.7	3	2	-1.016
10	ATM006.045	1992	109	09	35	56	1328.3	1438.2	1035.6	3	1	-0.916
11	ATM005.291	1988	336	05	26	28	1000.7	1850.8	972.6	3	3	-0.738
12	ATM005.233	1988	325	12	31	52	2512.3	2498.6	3286.3	3	3	-0.415
13	ATM005.205	1988	321	16	00	17	-609.3	2111.2	1343.6	3	3	0.567
14	ATM005.204	1988	320	21	53	08	-212.8	1611.3	1587.3	3	3	0.477
15	ATM005.178	1988	309	23	41	18	-563.0	1680.4	2429.6	3	3	0.373
16	ATM005.177	1988	309	22	43	46	1658.6	1711.5	648.0	3	3	-0.474
17	ATM005.168	1988	308	01	02	32	-193.6	1840.1	1773.8	3	3	0.381
18	ATM005.156	1988	303	10	46	07	928.0	1562.9	1138.3	3	2	-0.167
19	ATM005.119	1988	288	06	05	28	1208.9	1485.6	595.7	3	2	-0.541
20	ATM005.102	1988	277	12	10	51	1056.4	1215.7	816.5	3	3	-0.233
21	ATM005.101	1988	277	01	10	25	1314.6	1289.2	689.7	3	2	-0.644
22	ATM005.100	1988	277	01	04	23	1733.8	1199.6	1099.9	3	2	0.110
23	ATM005.027	1988	233	13	42	12	1385.8	1336.1	505.1	3	3	-0.821
24	ATM004.184	1988	98	14	13	31	974.4	2232.4	1174.1	3	1	-0.959
25	ATM004.133	1988	58	16	55	00	1704.93	1953.2	683.0	3	2	-0.672
26	ATM003.278	1987	230	18	11	32	2420.1	1332.9	868.6	3	1	-0.497
27	ATM003.276	1987	230	23	31	56	737.5	2163.7	827.0	3	2	0.977
28	ATM003.275	1987	230	19	24	48	1055.8	2019.8	609.5	3	2	0.364
29	ATM003.253	1987	219	14	00	33	1663.5	1707.7	600.2	3	3	-0.352
30	ATM003.252	1987	219	13	56	34	1563.5	1606.7	777.3	3	3	-0.770
31	ATM003.077	1987	144	00	12	41	2536.6	635.7	530.7	3	1	-1.250
32	ATM003.052	1987	135	04	09	42	2058.5	1595.1	836.9	3	2	-1.068
33	ATM002.407	1987	112	17	36	40	1738.2	1714.8	878.9	3	2	-0.570
34	ATM002.318	1987	85	21	14	16	797.3	1647.6	817.2	3	2	-0.909
35	ATM002.203	1987	77	14	04	22	1754.7	2480.6	1384.9	3	2	-0.628
36	ATM002.165	1987	75	02	05	06	2047.3	1324.8	1201.3	3	3	-0.114
37	ATM002.164	1987	73	04	41	30	1256.3	1450.6	712.1	3	2	-0.145
38	ATM002.152	1987	71	23	06	03	2070.5	544.9	1173.3	3	2	-0.585
39	ATM002.148	1987	71	19	56	44	277.8	2426.8	785.5	3	2	-0.809
40	ATM002.137	1987	68	03	35	29	1418.7	2016.1	514.7	3	3	-0.045
41	ATM002.132	1987	67	22	34	13	2096.7	1611.6	1256.3	3	3	-0.556
42	ATM002.099	1987	63	16	10	19	1791.7	1832.3	550.3	3	3	-0.752
43	ATM002.093	1987	61	07	05	04	1449.9	1336.2	749.1	3	3	-0.830
44	ATM002.053	1987	50	21	52	45	1407.5	1489.8	1194.6	3	3	-0.525
45	**ATM001.174B**	1986	336	14	46	54	1511.6	1549.1	851.1	3	2	-0.500
46	**ATM001.174A**	1986	336	14	46	52	1232.4	1432.5	942.6	3	2	-0.494
47	ATM001.163	1986	332	12	30	58	1431.4	1575.4	1011.4	3	3	0.131
48	ATM001.074	1986	320	04	00	29	1614.1	1630.0	880.6	3	3	-0.763